Suspensions of Silica Particles Grafted with Concentrated Polymer Brush: A New Family of Colloidal Crystals

Kohji Ohno, Takashi Morinaga, Satoshi Takeno, Yoshinobu Tsujii, and Takeshi Fukuda*

Institute for Chemical Research, Kyoto University, Uji, Kyoto 611-0011, Japan

Received October 7, 2005; Revised Manuscript Received November 14, 2005

ABSTRACT: A colloidal crystal was newly identified for a liquid suspension of the hybrid particles having a spherical silica core and a shell of well-defined poly(methyl methacrylate) "concentrated brush". With increasing particle concentration, the suspension progressed from a (disordered) fluid to a fully crystallized system, going through a narrow crystal/fluid coexisting regime. The crystal had a face-centered cubic structure with a surprisingly large nearest-neighbor interparticle distance, suggesting that the graft chains, highly extended due to the "concentrated brush effect", exerted a long-range steric interaction. This type of colloidal crystal is new with respect to the origin of long-range interparticle potential and the controllability of many of the system parameters.

Introduction

Colloidal crystals have attracted much interest not only as photonic materials[1−3] but also as a model system to investigate fundamentals of condensed matter crystallization.[4−16] Typical colloidal crystals are formed by spherical particles suspended in a liquid. At low particle volume concentration ϕ, such a suspension is a (disordered) fluid, while above a crystallization concentration ϕ_f, crystallites separate out from the fluid, and crystal and fluid phases coexist in thermodynamic equilibrium until the concentration reaches another critical value ϕ_m, above which the system is totally crystalline. Driving forces for the formation of colloidal crystals are believed to be repulsive potentials working between colloidal particles, of which essentially two types have been known so far. One is the hard-sphere potential, which is steric and short-range in nature, inducing crystallization of rigid uncharged particles ("hard" colloidal crystals).[6−9,12,13] The other is the electrostatic potential, which is of extremely long range depending on the ionic strength of the system, inducing crystallization of charged particles ("soft" colloidal crystals).[10,11,17,18] Reference values of ϕ_f and ϕ_m for hard systems are 0.494 and 0.545, respectively,[19] while typical values of ϕ_f or ϕ_m for soft systems are on the order of 0.01, even though they increase with increasing ionic strength.[11,18] In this report, we identify a third type of colloidal crystal, in which the interparticle potential is exerted by the steric or excluded-volume interactions between the "concentrated polymer brushes" chemically bound on the particle surfaces. These interactions can also be of very long range, giving a coexisting regime (ϕ_f or ϕ_m) situated between those of soft and hard systems in typical cases.

Concentrated polymer brushes, that is, films of polymer chains end-grafted on a solid surface with a very high surface density (typically, higher than a few tenths of chains per square nanometer), exhibit structure and properties largely different from those of "semidilute brushes" characterized by a lower graft density (low enough to be describable by the two-body intersegmental interaction theory).[20] In particular, we have shown that a concentrated poly(methyl methacrylate) (PMMA) brush formed on a silicon wafer is highly swollen in a good solvent to give a film thickness as large as 80−90% of the full contour length of the PMMA grafts,[21,22] suggesting that the chains are extended nearly as highly. We have also shown microtribologically that the friction coefficient between swollen concentrated brushes is extremely small *even at high pressures*, suggesting that concentrated brushes would hardly interpenetrate each other.[23] These are among the notable effects of concentrated brushes, not of semidilute brushes, which are presumed to originate in the extremely high osmotic pressure in the concentrated brush layer and the entropically unfavorable conformation of the highly extended chains. These findings have led us to postulate that concentrated brushes formed on spherical particles would also be highly swollen in a good solvent, exerting a quasi-hard-sphere potential of long range between particles. If so, such hybrid particles dispersed in a good solvent for the polymer brush can form a colloidal crystal at a concentration regime dependent on the chain length and density of the grafts. Of course, the effective graft density and hence the mentioned concentrated brush effects would decrease with increasing radial distance or increasing graft chain length relative to the particle radius. In this regard, too, the postulated interparticle potential cannot be a rigid one, and we would term it a "semisoft" potential. In what follows, we will demonstrate that the postulated phenomenon is observed for monodisperse silica particles (SiPs) grafted with a concentrated PMMA brush.

This type of hybrid particles should not be confused with previously studied ones, a typical example of which had a core of SiP and a shell of bulk PMMA, prepared by dispersion polymerization of methyl methacrylate (MMA) in the presence of SiP as a seed.[6] Another typical example had a core of SiP and a shell of short polyisobutene chains with an unknown graft density.[24,25] The polymer shell in the former system behaved just as a hard shell, as the particles were suspended in a nonsolvent for the shell polymer. The polymer layer in the latter system played the role of stabilizer to prevent aggregation of SiPs, making only a minor contribution to the interparticle potential. Note that the three-dimensionally ordered assemblies often formed by sedimentation of such or other fine particles in suspension or evaporation of suspending solvent should be distinguished from the hard and soft colloidal crystals mentioned above and the semisoft one presented here. The latter three systems are all substantiated by thermodynamic equilibrium.

* To whom correspondence should be addressed: e-mail fukuda@scl.kyoto-u.ac.jp.

10.1021/ma0521708 CCC: $33.50
Published on Web 12/31/2005

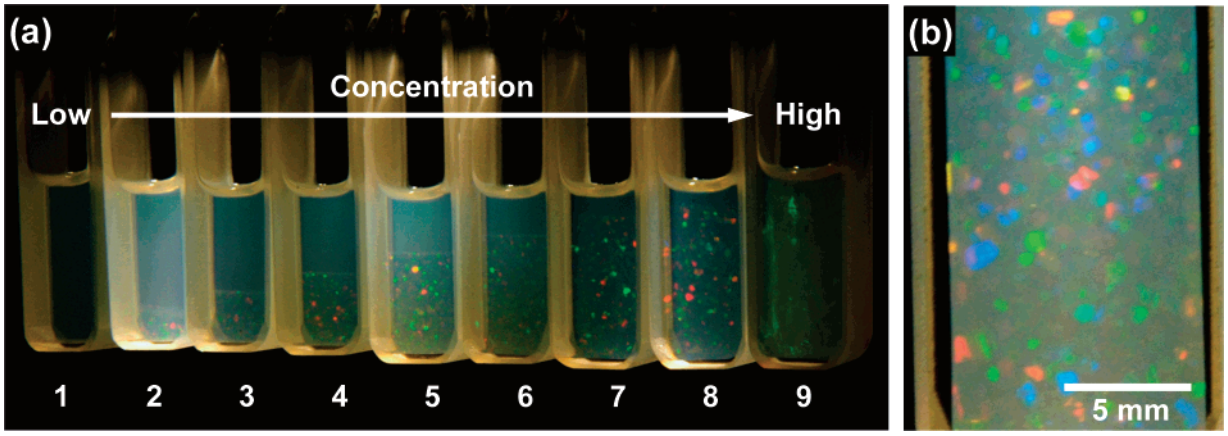

Figure 1. Photographs of PMMA-SiP suspensions in the mixed solvent (1,2-dichloroethane/chlorobenzene/*o*-dichlorobenzene = 53/20/27 volume ratio) illuminated from behind by white light, 7 days after sample preparation. The number-average molecular weight of the PMMA grafts is 158 000, and the diameter of the SiP core is 130 nm. (a) Samples with different PMMA-SiP volume fractions (ϕ). The ϕ value increases from 0.0785 (leftmost) to 0.111 (rightmost). In samples 2−8, Bragg-diffracting crystalline and (random) fluid phases coexist, with the volume fraction of crystalline phase increasing with increasing ϕ. Sample 9 ($\phi = 0.111$) crystallizes heterogeneously and sample 1 ($\phi = 0.0785$) remained unchanged (fluid phase). (b) Close-up of sample 8. The crystals are 0.1−1 mm in size, and show different colors depending on their orientation.

Also note that it was not until recently that we succeeded for the first time in preparing *perfectly dispersive*, nearly monodisperse fine particles grafted with a concentrated polymer brush.[26] In this regard also, this type of colloidal crystal is unprecedented.

Experimental Section

Materials. SiP (Seahoster KE-E10, 20 wt % suspension of SiP in ethylene glycol) was kindly donated by Nippon Shokubai Co., Ltd., Osaka, Japan. The mean diameter of the SiP was 130 nm with a relative standard deviation of 10%, as measured by transmission electron microscopy. The hybrid particles (PMMA-SiPs) were synthesized by surface-initiated atom transfer radical polymerization[27] of MMA, as reported previously.[26] They had the SiP core and a shell of PMMA chains with number-average molecular weight $M_n = 158\,000$ and polydispersity index $M_w/M_n = 1.19$, end-grafted on the SiP surface with a surface density as high as 0.70 chain/nm^2. These figures mean that each SiP had an average of 37 000 grafts. Knowing the weight fraction of PMMA in the hybrid particle and literature values of refractive index n and density ρ of PMMA and SiP in the bulk, we calculated the overall (average) refractive index and density of the PMMA-SiP hybrid particle to be 1.48 and 1.29 g/cm^3, respectively. 1,2-Dichloroethane (99.5%), chlorobenzene (99%), and *o*-dichlorobenzene (99%) were used as received from Nacalai Tesque Inc., Osaka, Japan.

Preparation of PMMA-SiP Suspensions. The PMMA-SiPs were dispersed in a mixture of 1,2-dichloroethane/chlorobenzene/*o*-dichlorobenzene of volume composition 53/20/27. The n and ρ values of this solvent mixture, approximated by composition averages of those of the pure solvents, are 1.49 and 1.24 g/cm^3, respectively, which are almost equal to those of the PMMA-SiP. The refractive index matching provides nearly transparent samples, and the density matching reduces the effect of gravity.[5−8]

Confocal Laser Scanning Microscopic Measurement of PMMA-SiP Suspensions. A PMMA-SiP suspension (0.3 mL) was put into a glass cell (0.8 cm in diameter and 1.5 cm in height) whose bottom was made of a coverslip and top was sealed by gluing a slide glass. Observation was made on an inverted type CLSM (LSM 5 PASCAL, Carl Zeiss, Germany) with a 458 nm wavelength Ar laser and 63× objective (Plan Apochromat, Carl Zeiss) in reflection mode. The distance of the focal plane from the inside surface of the coverslip was 100 μm.

Results and Discussion

PMMA-SiP suspensions in the solvent mixture with different particle volume fractions ($\phi = 0.0785-0.111$) were placed in Pyrex glass cells (10 × 10 × 40 mm) connected with a glass tube for sealing, and the systems were sealed off and allowed to stand at 25 °C for 7 days. Figure 1a shows the photographs of the series of samples illuminated from behind by white light. The numbers shown in Figure 1a represent the sample codes. In sample 1 with the lowest concentration examined here, the entire body of the suspension remained slightly turbid due to the Tyndall scattering. Sample 9 with the highest particle concentration exhibited heterogeneously iridescent colors within an hour after sample setting, which hardly changed throughout the experimental period of 7 days. In samples 2−8 with intermediate concentrations, tiny iridescent flecks were observed soon after the onset of experiment, indicating the formation of Bragg-reflecting crystallites. In sample 8, the formed crystallites filled the whole volume of the suspension from an early stage of experiment without sedimentation. In samples 2−7, as time elapsed, the crystallites sedimented under the effect of gravity, and the boundary between the iridescent-colored sediment (crystalline phase) and the slightly turbid supernatant (fluid phase) became more and more distinct, ultimately giving a sharp horizontal boundary line. This spontaneous phase separation can be interpreted by the idea of the Kirkwood−Alder transition.[19,28] The sedimentation of the crystalline phase occurs because the particle concentration (and hence the density) of the crystalline phase is slightly larger than that of the fluid phase.[7,9] Figure 1b shows a close-up of sample 8, which is composed of a pure crystalline phase. Single crystals 0.1−1 mm in size are visible, showing different colors depending on their orientations. Upon tumbling the cell, the iridescent colors observed in samples 2−8 instantaneously disappeared, and upon standing they appeared again in almost the same way as before.

Figure 2 shows a phase diagram constructed with the data shown in Figure 1a. In the coexistent region of fluid and crystalline phases, the plot shows a linear relationship. By extrapolating it to 0% and 100% crystal, we determined the freezing and melting volume fractions, ϕ_f and ϕ_m, to be 0.0795 and 0.0865, respectively. These values lie between the typical values for soft and hard colloidal crystals cited above. The relative width of the coexisting regime, $(\phi_m - \phi_f)/\phi_f = 0.088$, is slightly smaller than the value 0.103 for hard crystals (see above), presumably reflecting the difference in potential curve.

A PMMA-SiP suspension ($\phi = 0.087 > \phi_m$) was subjected to confocal laser scanning microscopic (CLSM) measurement to visually observe the crystal structure. Figure 3 shows a CLSM

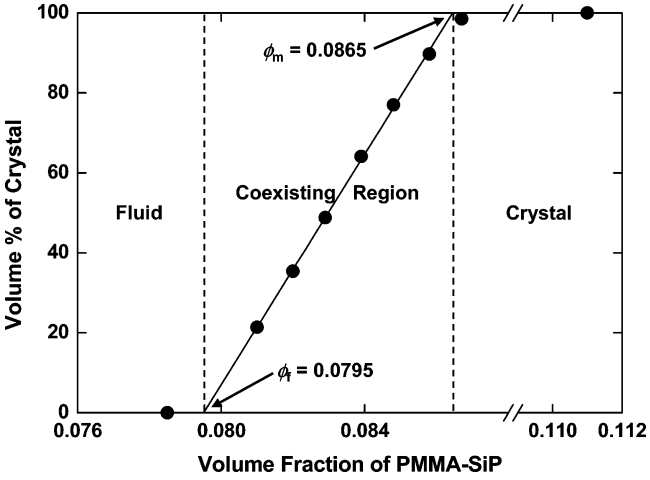

Figure 2. Phase diagram showing the volume fraction of crystal as a function of the particle volume fraction of PMMA-SiP suspension (data from Figure 1). By extrapolating the linear line observed for the coexisting region to 0% and 100% crystal, the freezing (ϕ_f) and melting (ϕ_m) volume fractions of the crystal were determined to be 0.0795 and 0.0865, respectively.

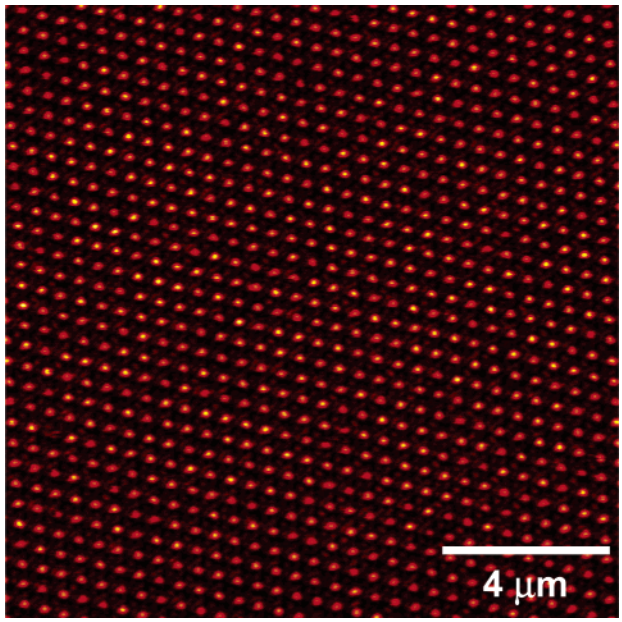

Figure 3. Confocal laser scanning microscopic images of PMMA-SiP crystals. Observations were performed with an Ar laser of 488 nm wavelength and ×63 objective in reflection mode. The distance of the focal plane from the inside of the coverslip was 100 μm. The diameter of SiP core is 130 nm. The number-average molecular weight of PMMA grafts is 158 000. The mean nearest-neighbor interparticle distance was 560 nm.

image of a two-dimensional slice in the sample bulk. The SiP cores of the hybrid particles are clearly visible as yellow circles forming a 2-D (two-dimensional) hexagonal array, while the PMMA brushes that should be surrounding the SiP cores are hardly visible because of their much lower reflectivity. The nearest-neighbor interparticle distance D measured 560 nm (Figure 4a). This value, while close to the hydrodynamic radius $D_h = 2R_h = 520$ nm (see below), is much larger than the diameter 260 nm of the "compact core−shell model"[29] (Figure 4b), which consists of a SiP core and a PMMA shell of the bulk density, and is as large as about 52% of the diameter 1070 nm (calculated from the M_w value of 188 000) of the "fully stretched core−shell model"[29] (Figure 4c), which consists of a SiP core and a PMMA shell whose size is equal to that of the PMMA chains radially stretched in all-trans conformation. This

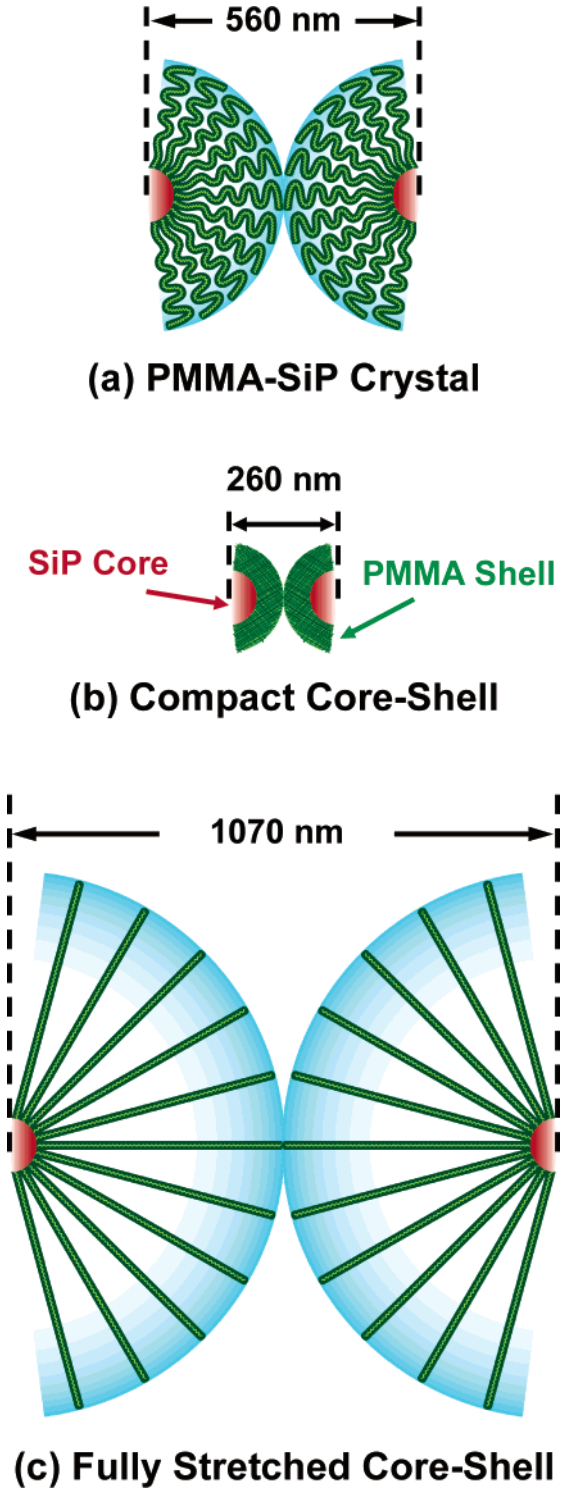

Figure 4. Schematic representations of polymer brush layers on silica particle surface of (a) PMMA-SiP crystal, (b) compact core−shell model, and (c)fully stretched core−shell model.

means that the PMMA shell is not compact but has a surprisingly large extension in the radial direction. (It is noteworthy that the unperturbed root-mean-square end-to-end distance L of PMMA chains of this molecular weight is only about 25 nm.[30])

Figure 5a−c shows the CLSM images of three successive $x-y$ layers in the same sample, each layer discriminated in a different color. These images were obtained by migrating the focal plane along the z-direction at a fixed $x-y$ position by $d = (2/3)^{1/2}D = 457$ nm, where d is the interlayer distance for

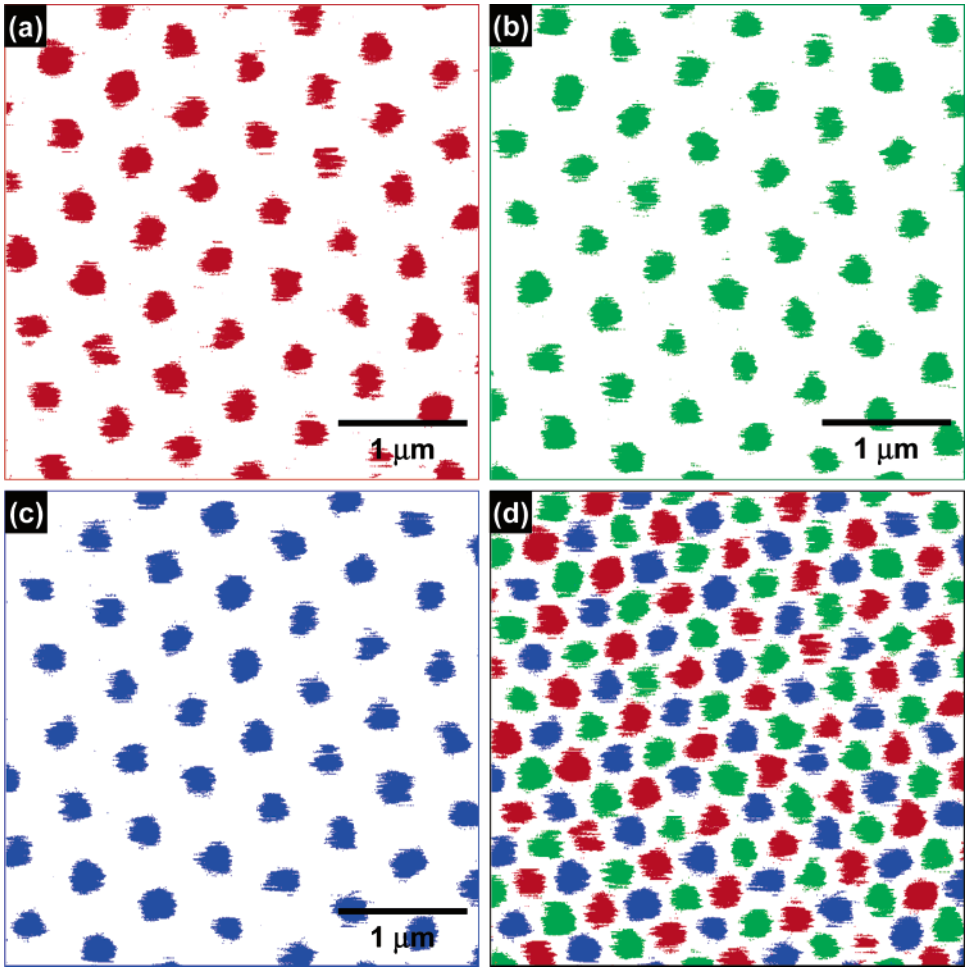

Figure 5. Structural analysis of PMMA-SiP crystal. The number-average molecular weight of the PMMA grafts is 158 000. **(**a−c**)** Confocal laser scanning microscopic images of $x-y$ slices for adjacent three layers of a crystal plane, discriminated in different colors. The three images were obtained by migrating the focal plane by $560(2/3)^{1/2} = 457$ nm in the z-direction at a fixed $x-y$ position. **(**d**)** Superposition of the three confocal micrographs in panels a−c. This represents the characteristic arrangement of the stacking of (1,1,1) planes in a face-centered cubic lattice.

both of the two possible lattices, that is, face-centered cubic (fcc) and hexagonal close-packed (hcp) lattices. All images show a 2-D hexagonal arrangement of particles. Figure 5d shows a superposition of these three images, where all particles are separately visible, just setting in the interstices, forming a new, smaller 2-D hexagonal array. This is the characteristic arrangement of an fcc lattice but not of an hcp one. Insofar as examined, admittedly limited, regions of the crystal are concerned, the present system is characterized by an fcc structure, not containing an hcp structure. It may be emphasized that we have for the first time succeeded in identifying the structure of a colloidal crystal formed by unlabeled (non-fluorescence-labeled) particles by using CLSM in reflection mode, although 2-D images of colloidal crystal had already been obtained by the same method.[31]

The volume fraction ϕ is the sum of those of the SiP core and the PMMA grafts. In the studied system, the SiP core contributes only about 13% to the total volume of the hybrid particle. The SiP and PMMA volume fractions at, for example, the melting point $\phi_m = 0.0865$ (see above) are $\phi_{m,SiP} = 0.011$ and $\phi_{m,PMMA} = 0.075$. This $\phi_{m,SiP}$ value is as low as for typical soft systems. The $\phi_{m,PMMA}$ value is also very small compared with the PMMA volume fraction of about 0.4 on the very surface of SiP core estimated from the graft density. The effective graft density and hence the concentrated brush effects would decrease with increasing radial distance from the core surface. According to the scaling theoretical picture, the end-to-end distance L of the brush chains on a flat surface shows different dependence on graft density σ below and above the crossover density σ_c.[32−35] In the semidilute regime ($\sigma < \sigma_c$), the mean distance between neighboring graft points, $\sigma^{-1/2}$, which measures the "blob" size, is large enough that the excluded-volume effect swells the blob, inducing a stretch of the chain given by $L \sim v^{1/3}N\sigma^{1/3}$, where N is the number of units per chain and v is the excluded-volume parameter ($v \ll 1$). In the concentrated regime ($\sigma > \sigma_c$), the blob size is so small that the excluded-volume effect is screened over the whole chain, giving a *higher* stretch, $L \sim N\sigma^{1/2}$. (In a previous paper,[22] we approximately demonstrated this behavior of concentrated brushes.) For chains end-grafted on a sphere of radius r_0 with a surface density σ_0, the effective surface density at a distance r from the sphere center will decrease with increasing r according to $\sigma(r) = \sigma_0(r_0/r)^2$. Hence these chains can exhibit a concentrated-to-semidilute conformational crossover along the chain contour, when both σ_0 and N are sufficiently large.[34,35] Our hybrid particle has $r_0 = 65$ nm, $\sigma_0 = 0.70$ chains/nm^2, and a hydrodynamic radius $R_h = 260$ nm (as determined by dynamic light scattering in tetrahydrofuran). Hence at $r = R_h$, we estimate $\sigma = 0.044$ chain/nm^2, hence $\sigma^{-1/2} = 4.8$ nm. This blob size corresponds to a PMMA chain with a molecular weight about 10 000 and is small enough to neglect the excluded-volume effect, suggesting that at least the main body of the brush chain is in the concentrated regime. This

discussion is also supported by the previous experiments (see Figures 5 and 6 in ref 22, showing the thickness vs σ relationship for PMMA brushes).

A particle coated with such a thick concentrated brush layer is new. The interparticle potential between them should be more of a hard-sphere nature than those between semidilute or dilute brushes or those having a concentrated-to-semidilute crossover. Work is in progress to study the dilute solution properties, crystallization, and crystalline structures of SiP−PMMA hybrid particles as a function of chain length and brush density. It will provide interesting materials to be discussed in more detail, in comparison with dilute solution theories,[34,35] crystallization theories and simulations,[36] and experiments with other relevant systems of interest, in particular, block copolymer micelles.[37]

Conclusions

Monodisperse SiP grafted with a concentrated PMMA brush layer and suspended in a good solvent of PMMA formed a colloidal crystal in a certain concentration range. Unlike the previously known (soft and hard) colloidal crystals, the driving force of crystallization in this system is a long-range repulsive (noninterpenetrating) interaction between the highly swollen concentrated brush layers. The crystallization concentration is situated between those of typical soft and hard systems. Hence this is a new type of colloidal crystal, which we would term a semisoft system. Main advantages of this system over the conventional ones include (1) controllability of the interparticle distance by controlling the graft chain length and density, (2) applicability to various monomers to have various graft polymers (e.g., hydrophilic, hydrophobic, and electrolytic polymers), (3) applicability to various particles (organic, inorganic, and metallic particles), and (4) usability of various solvents and solvent mixtures to adjust refractive index, light and X-ray absorbance, and density. We should add the comment that advantage 2 also suggests the possibility of fixation of the colloidal crystal by, for example, cross-linking all or a part of the graft layers via the cross-linkable units introduced in the graft chain. These advantages will offer unique possibilities for fundamental and applied research for colloidal crystals.

Acknowledgment. This work was supported in part by a Grant-in-Aid for Scientific Research (Grant-in-Aid 17002007 and 17685010) from the Ministry of Education, Culture, Sports, Science, and Technology, Japan, and by Industrial Technology Research Grant Program in 2004 from the New Energy and Industrial Technology Development Organization (NEDO) of Japan. We thank Nippon Shokubai Co. Ltd. for their kind donation of silica particle.

References and Notes

(1) Yablonovitch, E. *Nature* **1999**, *401*, 539−541.
(2) Arsenault, A.; Fournier-Bidoz, S.; Hatton, B.; Míguez, H.; Tétreault, N.; Vekris, E.; Wong, S.; Yang, S. M.; Kieaev, V.; Ozin, G. A. *J. Mater. Chem.* **2004**, *14*, 781−794.
(3) Colvin, V. L. *MRS Bull.* **2001**, *26*, 637−641.
(4) Habdas, P.; Weeks, E. R. *Curr. Opin. Colloid Interface Sci.* **2002**, *7*, 196−203.
(5) Yethiraj, A.; van Blaaderen, A. *Nature* **2003**, *421*, 513−517.
(6) Kegel, W. K.; van Blaaderen, A. *Science* **2000**, *287*, 290−293.
(7) Pusey, P. N.; van Megen, W. *Nature* **1986**, *320*, 340−342.
(8) van Megen, W.; Underwood, S. M. *Nature* **1993**, *362*, 616−618.
(9) Kose, A.; Hachisu, S. *J. Colloid Interface Sci.* **1974**, *46*, 460−469.
(10) Hachisu, S.; Kobayashi, Y.; Kose, A. *J. Colloid Interface Sci.* **1973**, *42*, 342−348.
(11) Hachisu, S.; Takano, K. *Adv. Colloid Interface Sci.* **1982**, *16*, 233−252.
(12) Cheng, Z.; Russel, W. B.; Chaikin, P. M. *Nature* **1999**, *401*, 893−895.
(13) Zhu, J.; Li, M.; Rogers, R.; Meyer, W.; Ottewill, R. H.; STS-73 Space Shuttle Crew; Russel, W. B.; Chaikin, P. M. *Nature* **1997**, *387*, 883−885.
(14) Auer, S.; Frenkel, D. *Nature* **2001**, *409*, 1020−1023.
(15) Gasser, U.; Weeks, E. R.; Schofield, A.; Pusey, P. N.; Weitz, D. A. *Science* **2001**, *292*, 258−262.
(16) Gast, A. P.; Monovoukas, Y. *Nature* **1991**, *351*, 553−555.
(17) Hiltner, P. A.; Krieger, I. M. *J. Phys. Chem.* **1969**, *73*, 2386−2389.
(18) Okubo, T. *Prog. Polym. Sci.* **1993**, *18*, 481−517.
(19) Hoover, W. G.; Ree, F. H. *J. Chem. Phys.* **1968**, *49*, 3609−3617.
(20) Advincula, R. C., Brittain, W. J., Caster, K. C., Rühe, J., Eds. *Polymer Brushes*; Wiley−VCH: Weinheim, Germany, 2004.
(21) Yamamoto, S.; Ejaz, M.; Tsujii, Y.; Matsumoto, M.; Fukuda, T. *Macromolecules* **2000**, *33*, 5602−5607.
(22) Yamamoto, S.; Ejaz, M.; Tsujii, Y.; Fukuda, T. *Macromolecules* **2000**, *33*, 5608−5612.
(23) Tsujii, Y.; Okayasu, K.; Ohno, K.; Fukuda, T. *Polym. Prepr. (Am. Chem. Soc., Div. Polym. Chem.)* **2005**, *46* (2), 85−86.
(24) Pathmamanoharan, C. *Colloids Surf.* **1988/89**, *34*, 81−88.
(25) Smits, C.; Briels, W. J.; Dhont, J. K. G.; Lekkerkerker, H. N. W. *Prog. Colloid Polym. Sci.* **1989**, *79*, 287−292.
(26) Ohno, K.; Morinaga, T.; Koh, K.; Tsujii, Y.; Fukuda, T. *Macromolecules* **2005**, *38*, 2137−2142.
(27) (a) Ejaz, M.; Yamamoto, S.; Ohno, K.; Tsujii, Y.; Fukuda, T. *Macromolecules* **1998**, *31*, 5934−5936. (b) Husseman, M.; Malmström, E. E.; McNamara, M.; Mate, M.; Mecerreyes, D.; Benoit, D. G.; Hedrick, J. L.; Mansky, P.; Huang, E.; Russell, T. P.; Hawker, C. J. *Macromolecules* **1999**, *32*, 1424−1431. (c) Matyjaszewski, K.; Miller, P. J.; Shukla, N.; Immaraporn, B.; Gelman, A.; Luokala, B. B.; Siclovan, T. M.; Kickelbick, G.; Vallant, T.; Hoffmann, H.; Pakula, T. *Macromolecules* **1999**, *32*, 8716−8724. (d) Jeyaprakash, J. D.; Samuel, S.; Dhamodharan, R.; Rühe, J. *Macromol. Rapid Commun.* **2002**, *23*, 277−281. (e) Mori, H.; Boker, A.; Krausch, G.; Müller, A. H. E. *Macromolecules* **2001**, *34*, 6871−6882. (f) Kim, J.-B.; Bruening, M. L.; Baker, G. L. *J. Am. Chem. Soc.* **2000**, *122*, 7616−7617. (g) Sedjo, R. A.; Mirous, B. K.; Brittain, W. J. *Macromolecules* **2000**, *33*, 1492−1493. (h) von Werne, T.; Patten, T. E. *J. Am. Chem. Soc.* **1999**, *121*, 7409−7410. (i) Perruchot, C.; Khan, M. A.; Kamitsi, A.; Armes, S. P.; von Werne, T.; Patten, T. E. *Langmuir* **2001**, *17*, 4479−4481. (j) Huang, X.; Wirth, M. J. *Anal. Chem.* **1997**, *69*, 4577−4580. (k) Jones, D. M.; Brown, A. A.; Huck, W. T. S. *Langmuir* **2002**, *18*, 1265−1269.
(28) Alder, B. J.; Hoover, W. G.; Young, D. A. *J. Chem. Phys.* **1968**, *49*, 3688−3696.
(29) Ohno, K.; Koh, K.; Tsujii, Y.; Fukuda, T. *Angew. Chem., Int. Ed.* **2003**, *42*, 2751−2754.
(30) Brandrup, J., Immergut, E. H., Grulke, E. A., Eds. *Polymer Handbook*, 4th ed.; John Wiley & Sons: New York, 1999; p VII/52.
(31) Yoshida, H.; Yamanaka, J.; Koga, T.; Ise, N.; Hashimoto, T. *Langmuir* **1998**, *14*, 569−574.
(32) Alexander, S. *J. Phys. (Paris)* **1977**, *38*, 983−987.
(33) de Gennes, P. G. *Macromolecules* **1980**, *13*, 1069−1075.
(34) Daoud, M.; Cotton, J. P. *J. Phys. (Paris)* **1982**, *43*, 531−538.
(35) Birstein, T. M.; Zhulina, E. B. *Polymer* **1984**, *25*, 1453−1461.
(36) Watzlawek, M.; Likos, C. N.; Löwen, H. *Phys. Rev. Lett.* **1999**, *82*, 5289−5292.
(37) (a) McCornnell, G. A.; Gast, A. P.; Huang, J. S.; Smith, S. D. *Phys. Rev. Lett.* **1993**, *71*, 2102−2105. (b) McCornell, G. A.; Gast, A. P. *Macromolecules* **1997**, *30*, 435−444.

MA0521708